3

Studies on graphene oxide and alkoxysilane functionalized PdNPs for the fabrication of silica-alginate beads: Catalyst for selective decomposition of hydrazine to hydrogen

Hydrogen is considered a requisite energy source for future perspectives, as it is a clean and inexhaustible fuel (Li et al., 2015; Chen et al., 2010; Chen et al., 2012). Besides having an edge over nonrenewable energy resources, efficient storage and utilization of hydrogen is still a challenging task. Recently various technological innovations are done to store the hydrogen energy (Singh and Xu, 2013). Hydrous hydrazine (N_2H_4) which consists of nearly 8.0 wt% of hydrogen is liquid over a range of temperature (298–343 K) and less vulnerable to explosion, therefore, it is considered a promising material for chemical hydrogen storage and transportation (Orimo et al., 2007; Yadav and Xu, 2012). Efficient and selective catalysts are required for on-board generation of hydrogen gas from hydrazine. Catalyst reinforced liberation of hydrogen on the decomposition of hydrazine (Singh et al., 2011) is one of the recent major findings. A number of catalysts have been fabricated for the decomposition of hydrazine till date, among them nanoscaled supported catalysts [FeNi/Cu, Ni (100), Ir-MWNTs], nanoparticle catalysts have gained much attention (Singh et al., 2009; Liu et al., 2010; Bunker and Smith, 2011; Manukyan et al., 2014; Oliaee et al., 2016). Although, these catalysts have been reported to attain 100% H_2 selectivity but almost in every case, decomposition occurred at higher

temperature (Singh and Xu. 2009; Wang et al., 2012). Graphene oxide (GO) based noble metal nanohybrids (Yang et al., 2009; Choi et al., 2011; Kim et al., 2012) are helpful in eliminating the dispersibility and electron transfer related issues (Geim and Novoselov, 2007; Xue et al., 2012; Tan et al., 2013; Hong et al., 2010; Fang et al., 2016; Tsen et al., 2012). The active sites of GO prevent the aggregation of nanocrystals and control the nano geometry (Yang et al., 2009; Choi et al., 2011; Kim et al., 2012; Gao et al., 2016; Jang et al., 2013; Qian et al., 2013; Muszynski et al., 2008; Xu et al., 2008). However, despite the high catalytic potential of GO based noble metal catalysts, efforts are being applied to either lower the concentrations of noble metal (Bunker and Smith, 2011) or design noble metal-free catalysts, which are economically viable.

To address these issues, recently the nanocatalysts are entrapped in the polymer matrix of calcium alginate beads, which provide immense dispersibility, and overcome the aggregation related problems which arise specifically due to the high mobility of particles (Bezbaruah et al., 2009; Kim et al., 2010; Pangkongadisak et al., 2014; Kuang et al., 2015). Due to the porous nature of beads, millions of nanoparticles can be enclosed into them. However, there is a possibility of leaching of the material from such polymeric systems, since the pore sizes are of the order, 6–16 nm (Bezbaruah et al., 2009). Thus, porosity order of gel beads is not compatible for retaining the nanoscale materials lying between 1 and 10 nm, which limit their operational activity over time. This chapter reports the encapsulation of alkoxysilane (EETMS, GPTMS) functionalized palladium nanoparticles into hydrogel beads to obtain silica alginate composite beads, which is investigated as a catalyst for hydrazine decomposition. It is observed that, ~100 ppm concentration of palladium per bead effectively decomposes about several thousand folds higher concentration of hydrazine solution (1.19 M), within finite time (5 s), which renders the

silica alginate bead encapsulated with palladium nanocomposites, as cost-effective catalyst for hydrogen evolution.

The maximum pore size of the calcium alginate beads ranging from 6 to 16 nm, (Bezbaruah et al., 2009) restricts the encapsulation of nanocrystals of 6 and below 6 nm, but the introduction of alkoxysilanes into the polymeric matrix of calcium alginate beads due to the specific properties of alkoxy group that allow the formation of –Si–O–Si– linkages within alginate matrix enabling precise control over the pore size through sol–gel processing (Brunel et al., 2000). This facilitates the loading of nanomaterials effectively and favors the generation of catalytically efficient silica-alginate mesoporous material. The functional ability of such alkoxysilanes allow the reduction of noble metal ions as reported earlier (Pandey and Singh, 2014; Pandey and Pandey, 2016a; Pandey et al., 2016; Pandey and Pandey, 2016b) and also discussed in chapter II.

The palladium nanoparticle (PdNPs) suspension is homogenized with sodium alginate solution that may permit the formation of mesoporous silica-alginate beads with variable concentration of alkoxysilanes as a result of complex interlocking between both the constituents. The mesoporous structure of silica-alginate beads is further be manipulated by introducing GO (Zhang et al., 2014). The in-situ growth of PdNPs on active sites of graphene sheets, led to the improvement in surface properties an also the catalytic potential of nanocrystals was equally enhanced. The composition of precursors was tailored to yield four different types of silica alginate beads namely; (1) Pd/EETMS, (2) Pd/GO/EETMS, (3) Pd/GPTMS, and (4) Pd/GO/GPTMS. Composite beads loaded with four types of palladium nanocomposites are examined for their catalytic ability towards the decomposition of hydrazine. Kinetics of hydrazine decomposition based on FTIR study, justified the decomposition of N–N bond of the same (Pandey and Pandey,

2016b). Almost complete decomposition occurred at room temperature with 100% H_2 selectivity without any appearance of ammonia in the spectra. Moreover, the amount of hydrogen released is reviewed using simple volumetric measurements, where MB rapidly converts to colourless reduced leuco form i.e., leucoMB, on combining with equimolar concentrations of hydrogen gas (Seo et al., 2012). Since the hydrogen gas is a reducing agent, thus the hydrogen evolved in the reaction is utilized for the reduction of nitro compounds like, p-nitroaniline (PNA) (Pozun et al., 2013; Gu et al., 2014). This also illustrates the rate of the decomposition of hydrazine in the presence of different composite beads. Densification of the porous structure of silica-alginate beads was examined through calcinations; subjection to these alterations led to the significant improvement in catalytic behavior toward hydrazine decomposition.

Also an attempt has been made to understand the role of graphene oxide in the preparation of 3-aminopropyltrimethoxysilane (APTMS) mediated gold nanoparticles (AuNPs). Graphene oxide induced synthesis of AuNPs led to the homogenous nucleation and stabilisation to give Au/GO nanohybrids. According to this process, the synthesis of gold nanoparticles took 2–3 min in relation to the time taken in the preparation without the intervention of graphene (Cui et al, 2015; Goncalves et al., 2009). The previous investigations on the conversion of APTMS capped gold cations into AuNPs in the presence of formaldehyde (Pandey and Chauhan, 2012; Pandey and Pandey, 2014a; Pandey et al., 2014b; Pandey et al, 2014c) yielded the AuNPs with the average diameter of 5–12 nm, (Halder et al., 2015; Perry et al., 2015; Dong et al., 2015) which was considerably large as compared to those of GO induced AuNPs ().

The findings on the formation and catalytic behavior of porous silica-alginate beads embodied with GO and EETMS/GPTMS based functionalized palladium nanocrystallites and the role of

graphene oxide (Xu et al., 2014; Halder et al., 2015; Fan et al., 2014; Chung et al., 2014) in the formation of Au/GO nanohybrids are reported herein.

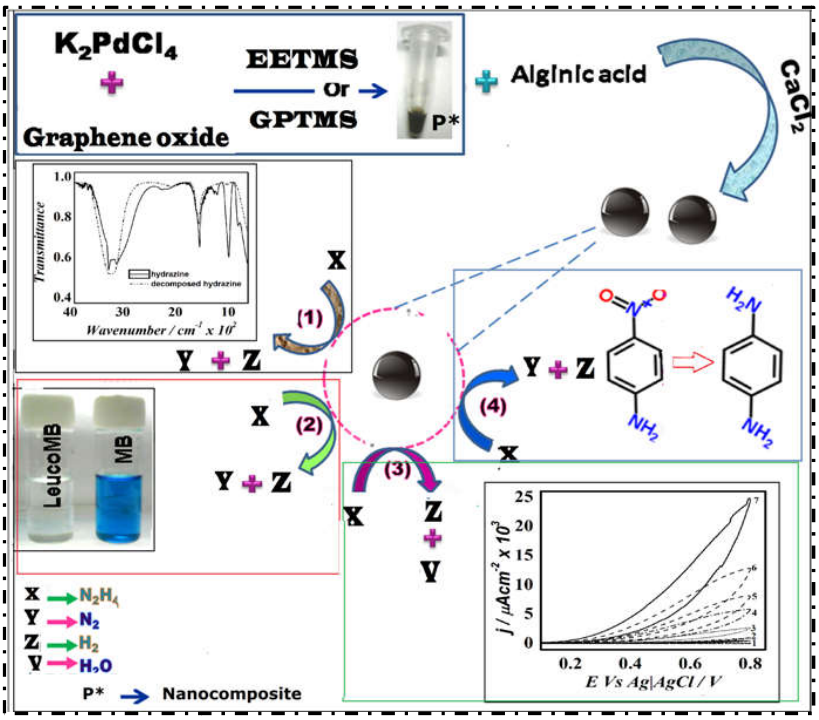

Scheme 3.1. Representation of experimental findings on synthesis of silica beads and catalysis, (1) evolution of hydrogen from N_2H_4 on reaction with silica alginate bead as catalysts, (2) conversion of MB to leucoMB in the presence of H_2, (3) electrocatalytic decomposition of N_2H_4 and (4) reduction of p-nitroaniline to p-diaminobenzene.

3.2. EXPERIMENTAL

3.2.1. Materials

Potassium tetrachloropalladate, 3-glycidoxypropyltrimethoxysilane (GPTMS), 2-(3,4-epoxycyclohexyl) ethyltrimethoxysilane (EETMS), 3-Aminopropyltrimethoxysilane (APTMS), tetrachloroauric acid, formaldehyde, polyvinylpyrrolidone (PVP), p-nitroaniline, sodium alginate

and calcium chloride were purchased from Sigma–Aldrich. The water used in all the experiments was Millipore double distilled water.

3.2.2. Synthesis of graphene oxide

Graphene oxide (GO) was synthesized using modified Hummer's approach (Hummers and R. E. Offeman, 1958; Sun et al., 2015). In brief, 0.3 g of graphite was added to a mixture of 2.4 mL 98% H_2SO_4, 0.5 g $K_2S_2O_8$, and 0.5 g P_2O_5, the contents were heated at 80 °C for 4 h.

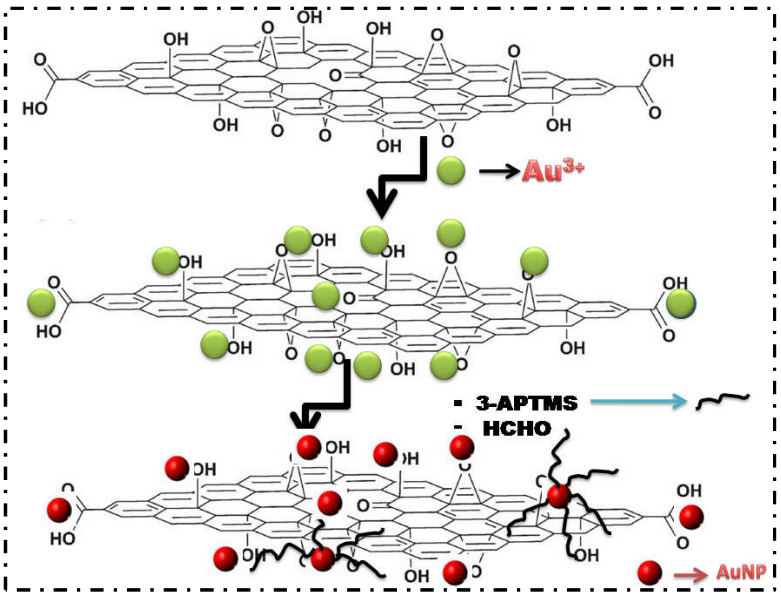

Scheme 3.2. Pictorial representation of the synthetic route of Au/GO nanohybrid.

The resulting product was washed with distilled water for a number of times and dried. Further, 12 mL of 98% H_2SO_4 was added to the preoxidized product, followed by addition of 1.5 g $KMnO_4$ maintained at below 20 °C in order to avoid overheating and explosion, the solution temperature was increased to 35 °C and maintained for 2 h, then 25 mL H_2O was added. After 2

h, additional 70 mL H_2O was added to dilute the solution and 2 mL of 30% H_2O_2 was injected into the solution to completely react with the excess $KMnO_4$. The bright yellow solution thus obtained was washed with HCl and H_2O, centrifuged and the residue was dried at 60 ºC.

3.2.3. Graphene oxide mediated synthesis of palladium nanoparticles

Firstly the Palladium nanoparticles (PdNPs), Pd/EETMS, and Pd/GPTMS were synthesized using chemical reduction method. In brief: to the 50 µL of 1 mM solution of K_2PdCl_4, the 10 µL of PVP solution was added, followed by the addition of 10 µL of 2.5 M solution of EETMS, the mixture was stirred and incubated for half an hour, brownish black dispersion of Pd/EETMS was obtained. Similarly, the Pd/GPTMS were synthesized using 50 µL of 1 mM K_2PdCl_4 solution, to which 50 µL of GPTMS was added. The mixture was stirred vigorously for 1 min and black colored suspension of Pd/GPTMS was obtained. Secondly, the obtained graphite oxide was dispersed in water and on sonication graphene oxide was achieved and Pd/GO (Pd/GO/EETMS and Pd/GO/GPTMS) nanocomposites were obtained as: 1 mg/mL dispersion of GO, to this 0.0032 g of K_2PdCl_4 was added to prepare 10 mM solution of Pd^{2+}/GO. Further, 50 µL of this mixture was used as Pd ion precursor, to which (a) 10 µL of PVP solution and 10 µL of 2.5 M EETMS were added, to obtain black colored Pd/GO/EETMS, while (b) 50 µL of GPTMS was added and mixed vigorously to obtain Pd/GO/GPTMS dispersion.

3.2.4. Fabrication of silica alginate beads and doping of nanocrystals

8 mg/mL solution of sodium alginate was prepared in distilled water. To this 400 µL solution, 200 µL of colloidal dispersion of palladium nanoparticles was added and the mixture was

sonicated for 30 min till the contents were homogenized. Dissolved 1.9 g of $CaCl_2$ in 20 mL of deionised water, and stirred for few minutes. Then by using a disposal syringe, filled with Pd/GO/alginate mixture, a fast stream was injected into the calcium chloride solution under the stirring conditions at room temperature, created a large number of beads. Resulting composite beads were separated out using fine sieves and washed with distilled water to remove extra calcium chloride and were stored at room temperature for use.

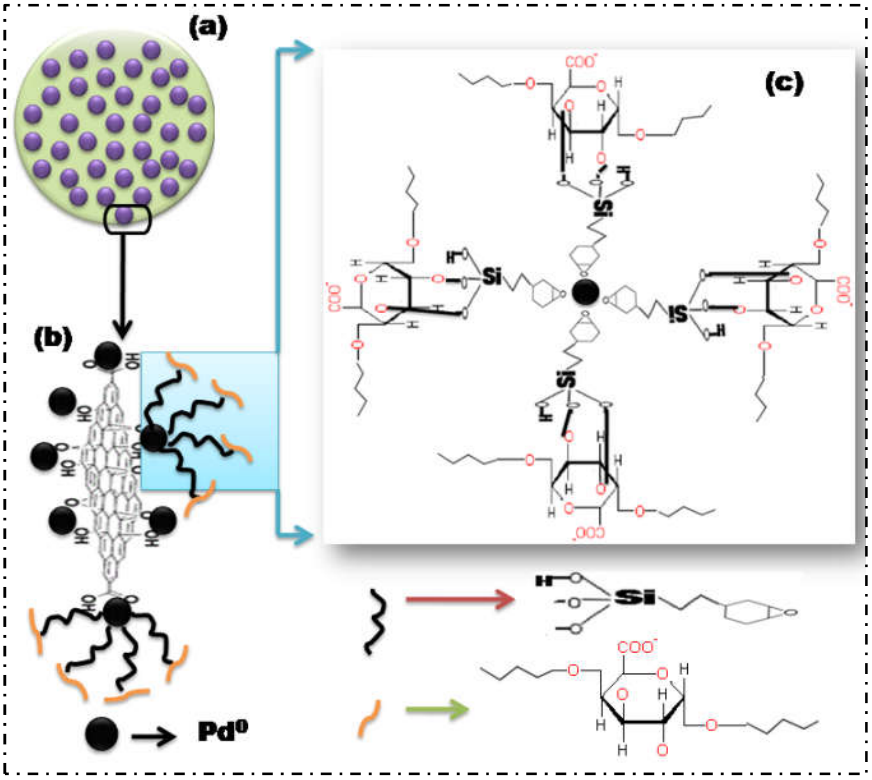

Scheme 3.3. Pictorial representation of interlinking between alkoxysilanes and polymeric chain of sodium alginate, (a) fabricated silica alginate beads, (b) shows the composition of bead, (c) possible chemical interactions between the precursors.

3.2.5. Synthesis of Au/GO nanohybrids

The synthesis of Au/GO nanohybrids, proceeds with the addition of 7.5 μL of APTMS to 94 μL of a 10 mg/mL suspension of GO, followed by sonication for 10 min to homogenise the contents. 40 μL of this mixture was added to 40 μL of 0.025 M ethanolic solution of chloroauric acid and the mixture was again sonicated for few minutes. The resulting mixture turned yellowish brown in color. 100 μL of formaldehyde was then added to this solution and was sonicated for about 10 min. On sonication, the mixture turned red indicating the formation of gold nanoparticles (AuNPs) as Au/GO nanohybrids.

3.2.6. Instrumentation

Transmission electron microscopy (TEM; Technai G2, 20 TWIN 50/60 Hz 210-240 V, 943205022121, FEI Czech Republic with accelerating voltage 200 kV) was used to evaluate the morphological features of as-synthesized nanocomposites. Colorimetric analyses were monitored using UV spectrophotometer (Hitachi U 2900, Hitachi Hi-Tech technologies, Tokyo Japan.). Measurements were done in 1 cm quartz cuvette in the wave length range of 200– 600 nm. FTIR analysis was carried out using Bruker, ALFA FTIR Bruker-ATR, Ettlington, Germany. HR-XRD (Smart SMART LAB, RIKAGU Corporation, 900 W, 45kV, 200 mA, target-Cu, detector- DTex Ultra 250, Akishima, Japan) was used to obtain diffractograms of the materials divulged to higher temperatures. SEM and EDX data obtained with ZEISS ZEISS EVO 18 Research, Germany). Zeta potential measurements were done using Brookhaven instrument.

3.3. RESULTS

3.3.1. Synthesis of palladium-GO nanocomposites

Alkoxysilanes are extensively investigated for their role in the synthesis of nanoparticles in the presence of another functional alkoxysilane as reducing agent (GPTMS) or small organic reducing agents [cyclohexanone, formaldehyde, tetrahydrofuran hydroperoxide (THF-HPO)] (Pandey and Singh, 2014; Pandey and Pandey, 2016a; Pandey et al., 2016; Pandey and Pandey, 2016b) as discussed in previous chapters. The synergistic co-operation between the functionalised matrix of GO, reducing and stabiling behavior of organically modified silanes, led to the conversion of PVP capped Pd^{2+} ions into clear and stable colloidal solutions of palladium nanocomposites (Liu et al., 2010; Bunker et al., 2011) namely Pd/GO/EETMS and Pd/GO/GPTMS. Figure 3.1 shows the absorbance spectra of PdNPs, synthesized using EETMS/GPTMS, in the presence and absence of GO.

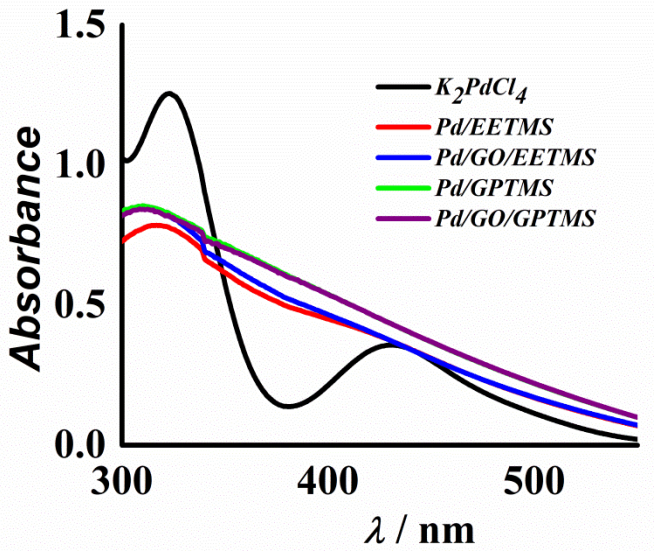

Figure 3.1. Absorbance spectra of conversion of Pd^{2+} to Pd^{0} under different conditions.

3.3.2. Characterisation of Pd/GO nanocomposites

FTIR spectra of Pd/GO/EETMS (Figure 3.2b) confirmed the presence of oxygen functionalities over the GO surface with bands at 3330.6 cm^{-1} due to C–OH stretching of hydroxyl or carboxylic functional groups, 1643.04 and 1016 cm^{-1} correspond to C=O streching and epoxy linkages (Paredes et al., 2008; Konios et al., 2014). Pd/EETMS nanoparticles are formed in clusters, as shown in Figure 3.3a, and have an average diameter of 13.4 ± 6.55 nm with broad distribution in particle sizes. On the other hand, the palladium nanocomposites modified with GO i.e., Pd/GO/EETMS (Figure 3.4a), are highly reduced in size with an average diameter of 3.41 ± 0.9 nm.

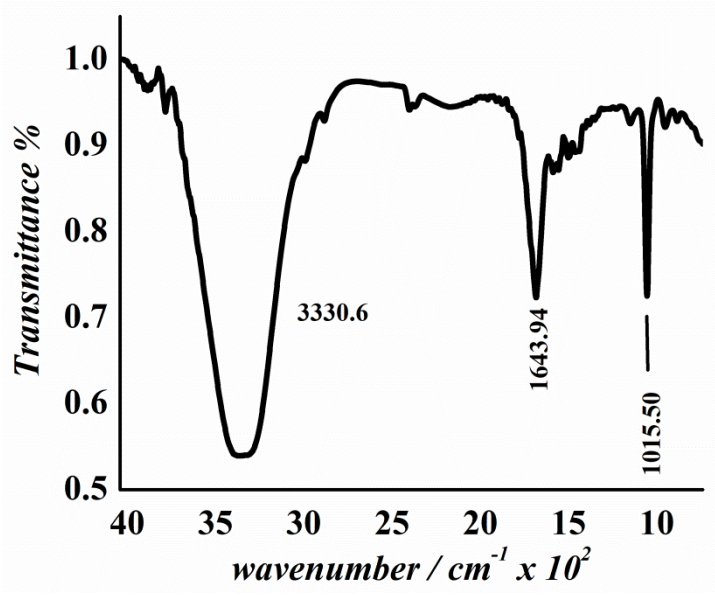

Figure 3.2. FTIR spectra of Pd/GO nanocomposite.

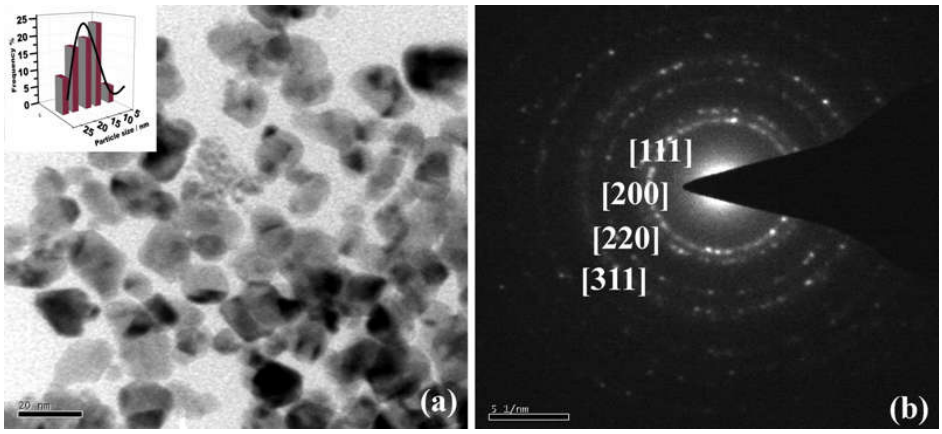

Figure 3.3. (a) TEM image, (b) descriptive SAED pattern of Pd/EETMS nanocomposites. Inset to picture (a) shows the corresponding size distribution.

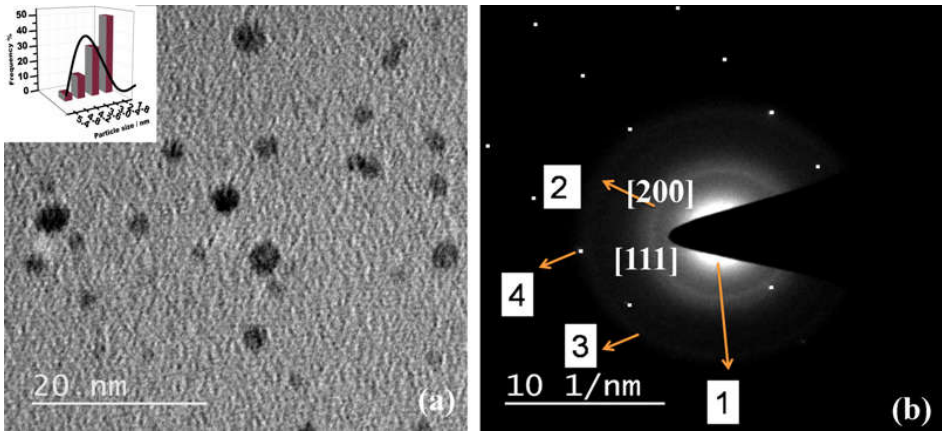

Figure 3.4. (a) TEM image, (b) descriptive SAED pattern of Pd/GO/EETMS nanocomposites. Inset to picture (a) shows the corresponding size distribution.

Similarly, palladium nanoparticles formed using GPTMS, i.e., Pd/GPTMS are found to be perfectly spherical with an average diameter of 3.8 ± 0.5 nm (Figure 3.5a), offering narrow particle size distributions (Figure 3.5).

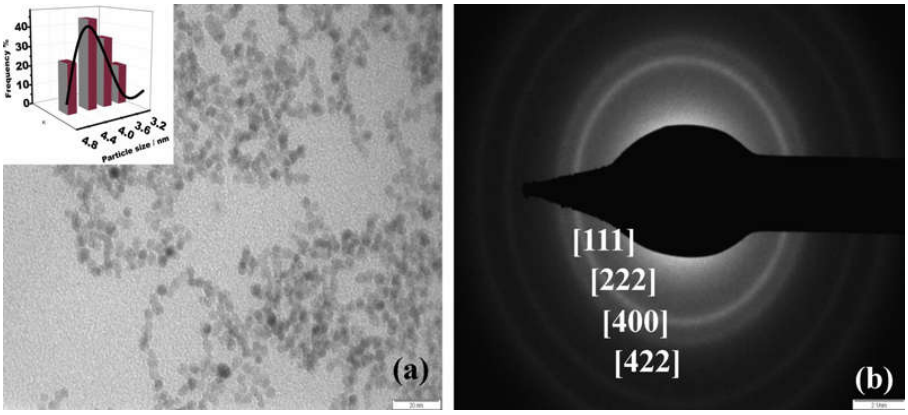

Figure 3.5. (a) TEM image, (b) descriptive SAED pattern of Pd/GPTMS nanocomposites. Inset to picture (a) shows the corresponding size distribution.

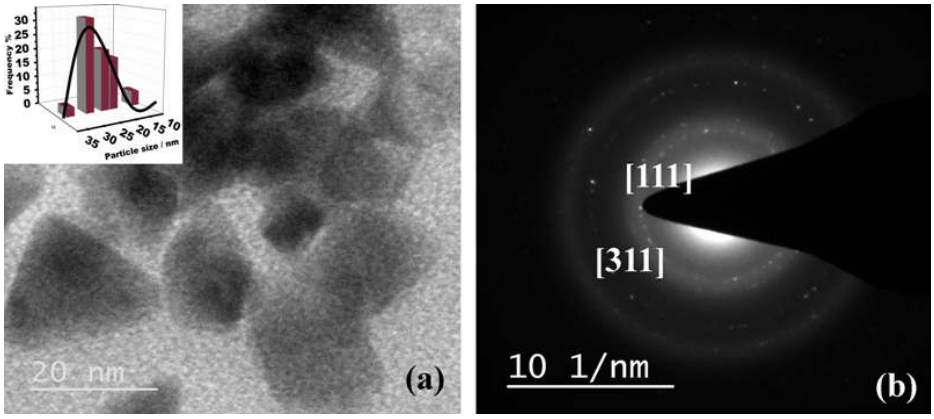

Figure 3.6. (a) TEM image, (b) descriptive SAED pattern of Pd/GO/GPTMS nanocomposites. Inset to picture (a) shows the corresponding size distribution.

The average diameter of these nanocomposites (Pd/GO/GPTMS) is observed to be 21.5 ± 7.4 nm (Figure 3.6a) in contrast to that obtained for the Pd/GO/EETMS nanocomposites. The polycrystalline growth of nanoparticles is confirmed by prominent concentric dotted ring pattern obtained for Pd/EETMS nanoparticles, indexed with the lattice planes (111), (200), (220), and (311) at corresponding d values given in Table 3.1, confirm the FCC arrangement. The electron

diffraction image of Pd/GPTMS showing the concentric rings indexed with lattice planes as (111), (222), (400), and (422).

3.3.3. Fabrication and characterization of mesoporous silica alginate beads doped with palladium nanocomposites

The reactive organic functionalities of alkoxysilanes tend to undergo specific interactions with polymer matrices through residual functional groups. Such compatible interactions lead to the evolution of novel composites, viable for different catalytic processes. Therefore; we have investigated the possibility of encapsulating the presynthesized alkoxysilane and graphene oxide stabilized palladium nanoparticles into the porous framework of calcium alginate matrix. The three dimensional matrix alginate polymers have been effectively used for loading zero valent species before (Bezbaruah et al., 2009). Palladium nanocomposite suspensions were found to disperse homogenously in the polymer matrix of alginic acid, which allow the encapsulation to form silica-alginate beads. Presently four types of palladium nanoparticles synthesized in a distinct manner (Pd/EETMS, Pd/GO/EETMS, Pd/GPTMS, and Pd/GO/GPTMS), are encapsulated into the silica beads. The surface properties of these nanoparticle entrapped silica alginate beads are analyzed using Scanning electron microscopy (SEM). The SEM image of the dried silica alginate beads shown in Figure 3.7a, presents a porous three dimensional surface, with interconnected pores. Figure 3.8b shows the corresponding EDX map of Pd/GO/EETMS nanocomposites containing silica alginate beads, displays the distribution of Pd in the ordered framework of beads. The average pore size of alginate gel beads has been recorded as 6–16 nm.

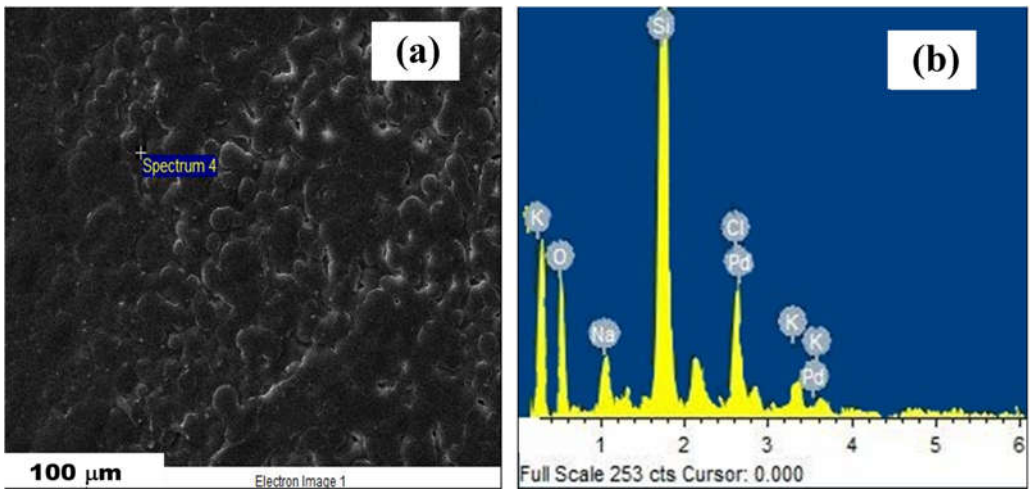

Figure 3.7. (a) SEM image of dried silica alginate beads entrapped with nanocomposites and (b) corresponding EDX map showing the distribution of the palladium in the beads along with Si and C.

3.3.4. Decomposition of hydrazine

The decomposition of hydrazine as a function of time was studied over different catalysts. Aliquots collected over fixed intervals of time were scanned within the range 3600–500 cm^{-1}. Band at 1069 cm^{-1} in IR spectra of hydrazine is due to N–N stretching disappears over time (Figure 3.8.a-c) which indicates the decomposition of hydrazine. The percentage conversion of hydrazine over Pd/GO/EETMS at 623 and 423 K, Pd/GO/EETMS, Pd/GO/GPTMS, Pd/EETMS, Pd/GPTMS at 300 K is obtained as 90–100%, 86%, 80%, 63%, and 45% Figure 3.9 over 1 h duration respectively. The decomposition rates were monitored using FTIR spectra. No sign of ammonia was observed in the IR spectra, confirming the complete decomposition of hydrazine into N_2 and H_2. Figure 3.10a-b shows the turn over frequencies (TOF) of different catalysts, which quantitatively defines their activity. The TOF values for different catalysts follow the

order: Pd/GO/EETMS (623 K) (300 h^{-1})> Pd/GO/EETMS (423 K) (270 h^{-1})> Pd/GO/ EETMS (230 h^{-1}) > Pd/GO/GPTMS (180 h^{-1}) > Pd/EETMS (150 h^{-1}) > Pd/GPTMS (80 h^{-1}) respectively.

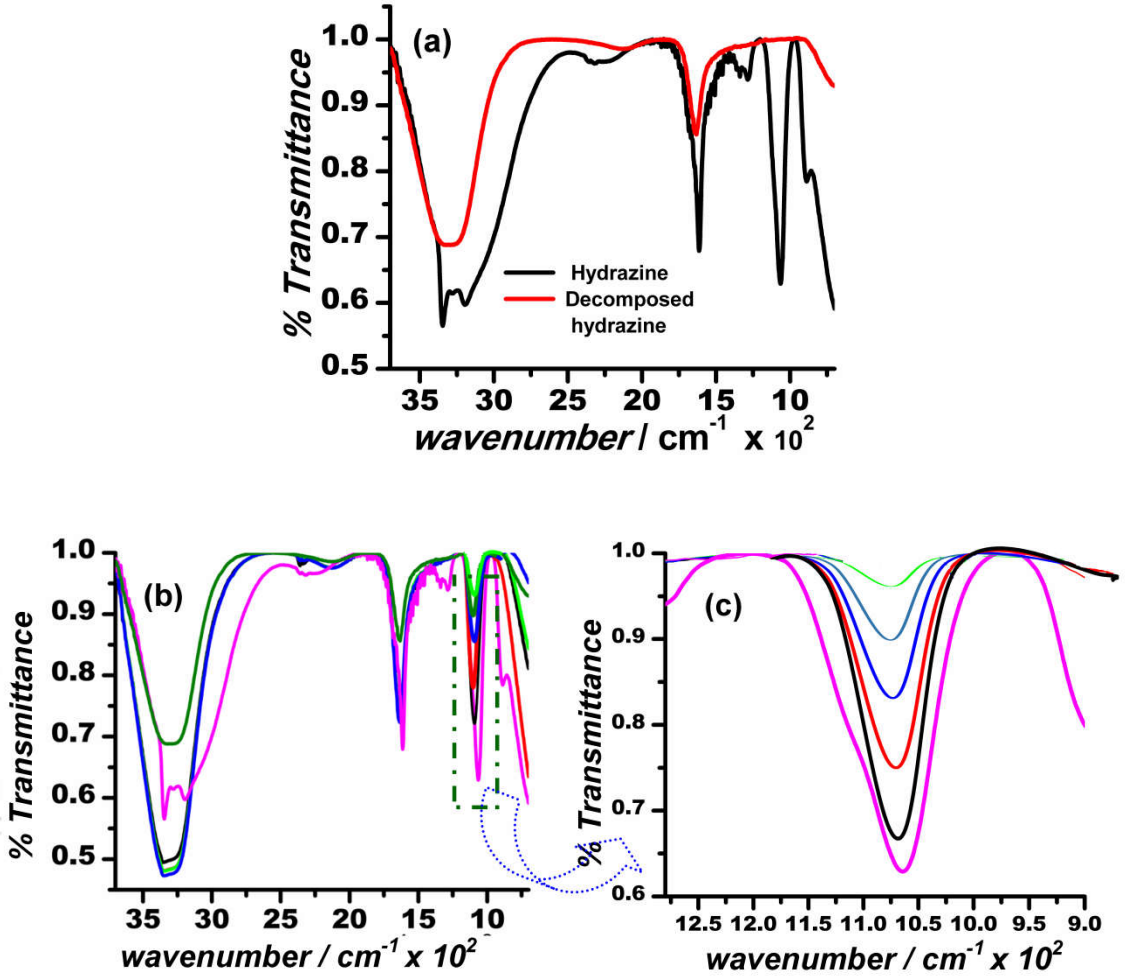

Figure 3.8. FTIR spectra of hydrazine solution before and after the decomposition (a), with time degradation of N–N bond stretching (b), magnified view of the dissipation of the band at 1069 cm^{-1} (c).

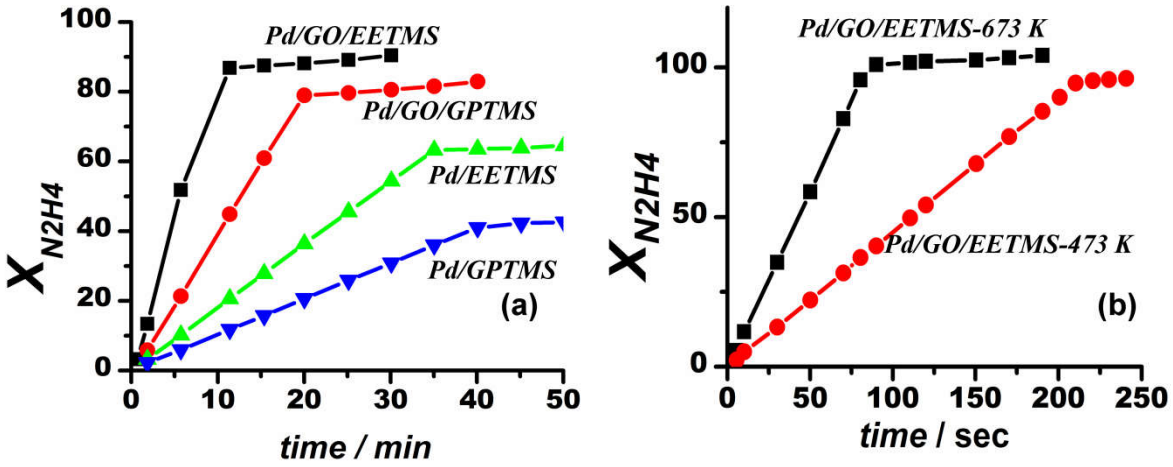

Figure 3.9. N_2H_4 conversion as a function of time using Pd/GO/EETMS (623 K), Pd/GO/EETMS (423 K), Pd/GO/EETMS, Pd/GO/GPTMS, Pd/EETMS, Pd/GPTMS catalysts at initial hydrazine concentration of 1.19 M.

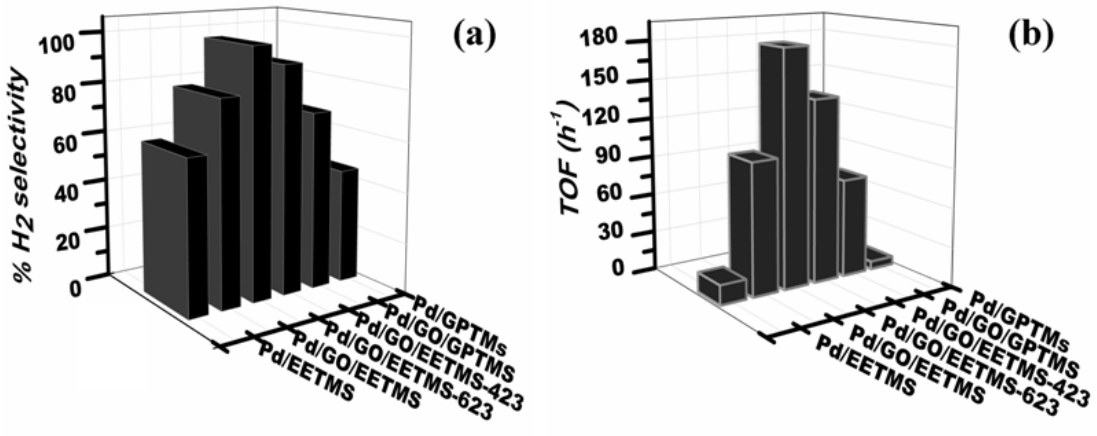

Figure 3.10. Comparative hydrogen selectivity of the prepared catalysts, TOF on decomposition of hydrazine by different catalysts.

3.3.5. Effect of heat treatment on catalytic activity

According to the hydrazine decomposition results, silica alginate beads with Pd/GO/EETMS are the most efficient catalyst among others, so in order to further understand the effect of densification on the catalytic performance, they were treated at elevated temperatures (up to 630 K), and examined for their catalytic potential thereafter. The calcinated catalyst responded even faster toward the decomposition of hydrazine (Figure 3.11), conversion of MB to leucoMB, reduction of p-nitroaniline to p-diaminobenzene.

3.3.6. Graphene oxide mediated synthesis and characterization of AuNPs

One-pot synthesis of Au/GO nanocomposites is demonstrated in two simple steps, whereby at first, graphene undergoes silanisation or chemical modification using an organofunctionalised silane, APTMS; second, the reduction of gold cations is achieved by applying a mild reducing agent, formaldehyde. The Au/GO nanohybrids are obtained by specific interaction between amino group of APTMS and graphene oxide sheets, which was confirmed by FTIR measurements. The characteristic absorption bands in the FTIR spectra (Figure 3.12) observed are: C–OH stretching at 3360.7 cm^{-1}, corresponding to hydroxyl groups and also due to the N–H stretching of APTMS, (Xue et al., 2012) either belonging to alcoholic or carboxylic functional groups; a band at 1646 cm^{-1}, relating to the sp^2 framework of graphene, and bands at 1093 cm^{-1}, 1017.73 cm^{-1} and 905 cm^{-1}, which refer to the C–O epoxy stretching (Konios et al., 2014; Paredes et al., 2008). The FTIR study confirmed the oxygen-functionalised nature of grapheme oxide as described in previous reports.

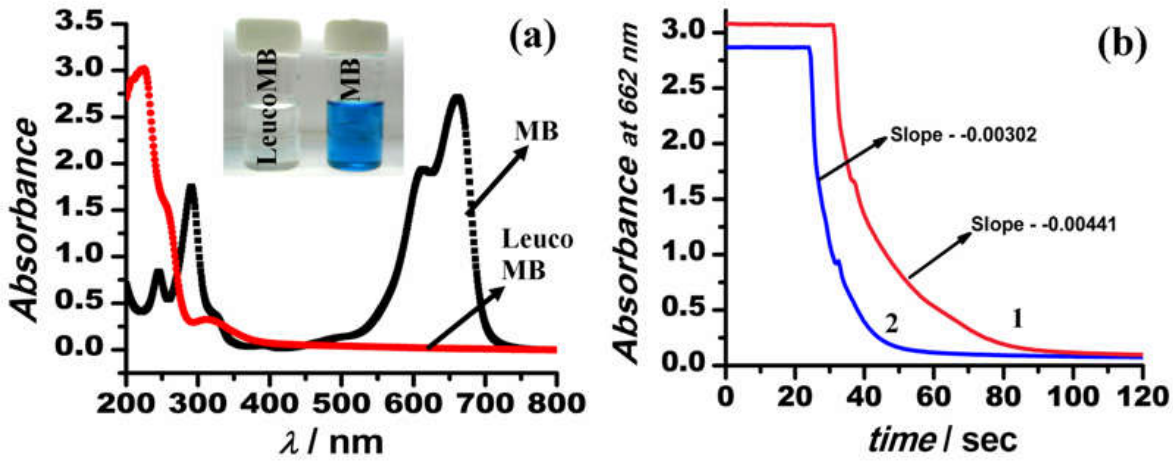

Figure 3.11. Absorbance spectra of the reduction of methylene blue (MB) to leucomethylene blue (leucoMB), (b) kinetic analysis of the process without (1) and with (2) temperature treatment of catalyst.

UV-Vis spectra of Au/GO nanocomposites showed a surface plasmon band at 515 nm as compared to AuNPs synthesized in absence of graphene oxide (Figure 3.12). There is red shift of about 15 nm in the case of AuNPs. The differences in absorbance predict the diversity in the number of nanoparticles in both cases. Transmission electron microscopic analysis of the nanocomposites reveals the presence of opaque and extremely fine sheets of graphene (Figure 3.13), and the successful loading of spherical gold nanocrystals in both cases (Au/GO and AuNPs). The diameters of the gold nanoparticles obtained were 2–5 nm in Au/GO and 7–9 nm (Figure 3.14) in the case of AuNPs. The mean spacing between the distinguished lattice fringes detected by HRTEM was nearly 0.330 nm (Figure 3.15). The average diameters of the Au/GO nanohybrids and AuNPs were 4.5 nm and 7.2 nm, respectively. The SAED patterns are well indexed with highly resolved lattice planes at corresponding d-values, namely, 0.230 nm (111), 0.201 nm (200), 0.14 nm (220), 0.095 nm (400), and 0.0798 nm (422) within Au/GO

nanohybrids, and 0.223 nm (111), 0.13 nm (220) and 0.121 nm (311) in the AuNPs. The lattice planes obtained here are in fair agreement with those reported in the literature.

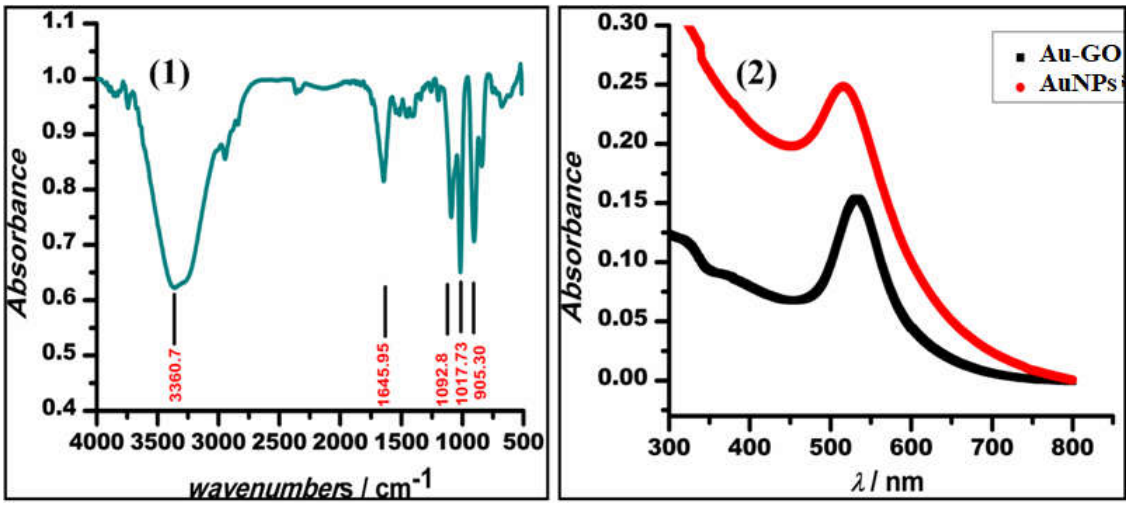

Figure 3.12. FTIR (1) and UV-Vis (3) spectra of Au/GO nanocomposite.

3.4. DISCUSSION

3.4.1. Synthesis and Morphological analysis of Pd/GO nanocomposites

Epoxy linkages present in both these alkoxysilanes are found to be reactive, (Darensbourg et al., 2003; Klein et al., 1983) which facilitates the conversion of metal ion to corresponding nanoparticles. The present process involves GO mediated synthesis of PdNPs. Oxygenated functional groups lying on the GO surface are negatively charged and they chemically assist the coupling of Pd ions (Pangkongadisak et al., 2014), with the 2D framework of GO sheets. Homogeneous colloidal solution of different types of palladium nanocomposites are formed, and their morphological features were studied using electron microscopy.

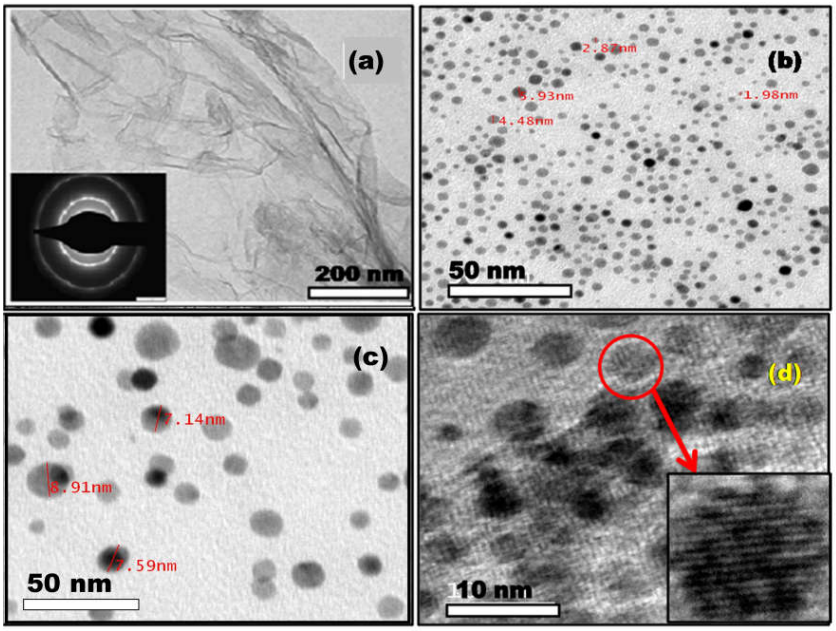

Figure 3.13. TEM images of graphene sheet (a), Au/GO nanohybrids (b) and (d), AuNPs (c) Inset to picture (a) shows the SAED pattern, and to (d) shows the magnified image of a nanoparticle with visible fringes.

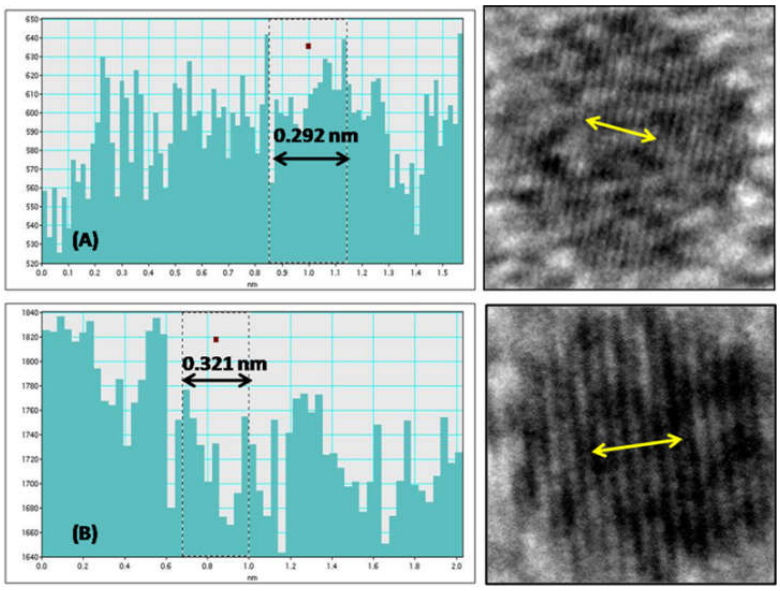

Figure 3.14. Plots showing the lattice spacings of Au–GO (A) and AuNPs (B).

The TEM images reveal the random orientation and angular shapes (viz, cubical, triangular, hexagonal) of Pd/GO/GPTMS nanoparticles and justify the consequence of synthetic procedure adopted during the synthesis. Such multiplicities observed in the nanogeometries of the nanocomposites are one of the factors which decides their differential catalytic behavior in various processes, discussed vide infra in the chapter. Selected area diffraction patterns of Pd/EETMS, Pd/GO/EETMS nanoparticles are shown in Figures 3.3 and 3.4. With the introduction of GO nanosheets in the synthesis of Pd/GO/EETMS nanomaterial, diffractogram shows a specific type of patterns as shown in Figure 3.4b. It consists of short, medium, and long range order, along with more than one or two phases. Different features in the SAED pattern are numbered, where 1—white hallow, confirming the presence of a ratio of the amorphous phase of the material. 2 and 3 are diffused rings suggesting the transformation to some degree of poly-crystallization phase 4—white spots confirm the presence of high crystalline phases. The two kinds of lattice planes obtained are (111) and (200) respectively.

On the other hand, diffractogram of Pd/GPTMS and Pd/GO/GPTMS are shown in Figures 3.5b and 3.6b respectively. Polycrystalline nature of the nanoparticles is proved from the complete and focused rings appeared. The GO doped nanoparticles (Pd/GO/GPTMS) displayed less defined dotted ring pattern along with the somewhat diffused area in the spectra revealing relatively less crystallinity as compared to that of Pd/GO/EETMS that contribute to the catalytic activity of as generated nanomaterials. Introduction of GO ensures the uniform distribution of nanoparticles as observed in case of Pd/GO/EETMS. However, in Pd/GO/GPTMS, heterogeneity is observed instead of the homogenous dispersion of the palladium nanocrystals over the graphene surfaces Figure 3.6. As generated palladium nanoparticles undergo interaction with

glycidoxy residue of GPTMS, which may not be allowing GO to show its usual behavior of controlling the nucleation of nanoparticle growth over its surface, resulting in such heterogeneity.

Table 3.1. Summary of values of d-spacing corresponding to the lattice planes obtained in synthesized Palladium nanocomposites.

Nanocomposites	**d [111]**	**d [200]**	**d [220]**	**d [222]**	**d [311]**	**d [400]**	**d[422]**
Pd/GPTMS	2.124	-	-	1.118	-	0.966	0.832
Pd/ EETMS	2.144	1.747	1.320	-	1.173	-	-
Pd/GO/EETMS	2.231	1.956	-	-	-	-	-
Pd/GO/GPTMS	2.102	-	-	-	1.170	-	-

3.4.2. Mesoporous silica beads preparation and characterisation

The polymer matrix and the presence of alkoxysilanes as one of the important constituent of the silica alginate beads, favors the formation of an interconnected network of the mesoporous bead. This property facilitates the generation of highly connected pore network, which in turn enhances the surface properties of the beads. Exploring such porous dimensions Bezbaruah, et al. (2009) encapsulated iron nanoparticles having average size of 35 nm within the porous alginate matrix for efficient applications (Bezbaruah et al, 2009). However, the size of as made palladium nanocrystallites lie between 3 and 7 nm, which may not be stable and are likely to leach out from the porous matrix.

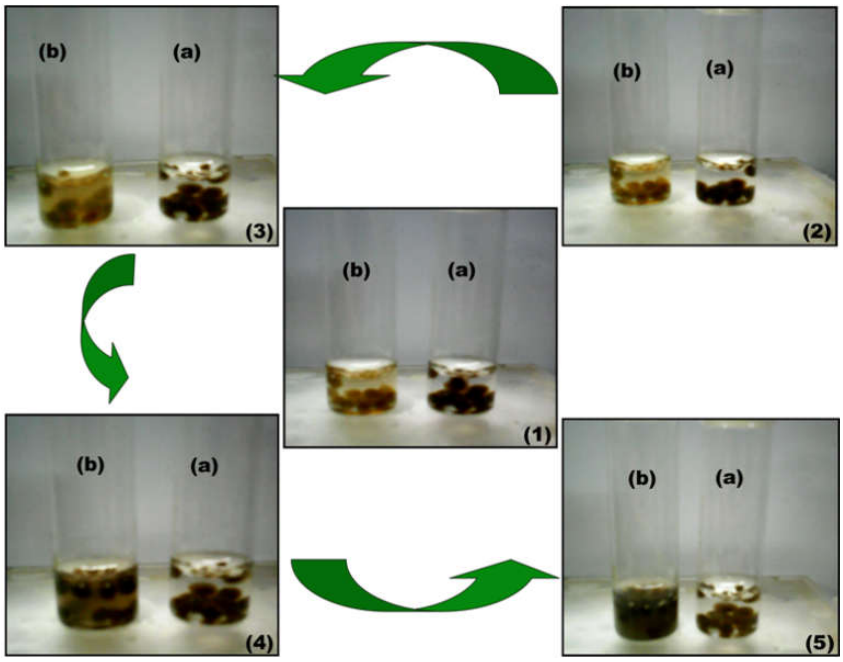

Scheme 3.4. Pictorial representation of the effect of concentration of alkoxysilanes on the porosity of silica beads. pictures 1-5 (anticlockwise), elucidates with time leaching of nanomaterial from the silica beads in case of lower content of alkoxysilanes (0.5 M) (b), in comparison to (a) where significant amount of alkoxysilane (2.5 M) is present.

The role of the concentration of alkoxysilane during the synthesis of alginate mesoporous beads has been studied, as a function of Si–O–Si linkages and van der Waals interactions between residual groups of polymer and alkoxysilane moieties, which persist at an optimum load of constituents. Scheme 3.3 shows the possible chemical interaction between the precursors of the silica-alginate beads scheme 3.1 shows the overview of all the experimental findings. At lower alkoxysilane content (0.5 M), the embedded colloidal dispersion of nanoparticles leaches out early, due to the less availability of interacting molecules as shown in scheme 3.4, weaker communications occur among the respective moieties. On increasing the concentration of alkoxysilanes (2.5 M), resulted in precise control over the compact and flexible character of silica alginate beads. Scheme 3.4 clearly elucidates the role of silica in the meticulous

arrangement of constituting segments, as the spilling out of material from silica beads is the measurement of the extent of interactions thus mesoporous character is achieved with the manipulations in the alkoxysilane content.

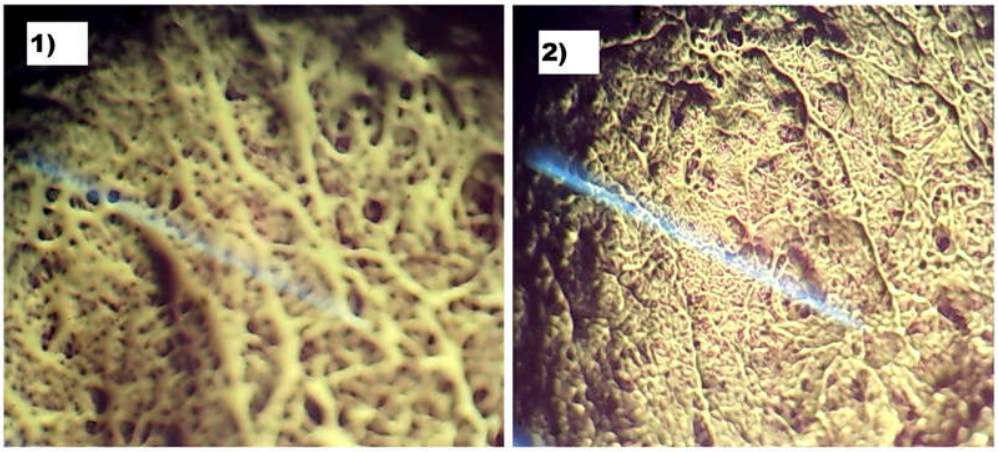

Figure 3.15. Optical micrographs showing the enlarged view of the silica beads, showing the variation in pore sizes with the concentration of silica, 1) 0.5 M and 2) 2.5 M.

Optical micrographs (Figure 3.15) show the magnified images of the silica beads, at two different concentrations of alkoxysilanes. Figure 3.15 shows the highly ordered and complicated frame-up of silica bead with smaller pore size, (to the order of 2–10 nm justifying the mesoporous framework suitable for encapsulation of nanoparticles for catalytic applications) in contrast to the one, where the concentrations of alkoxysilanes are low.

3.4.3. Fabrication Au/GO nanohybrid

APTMS was functionally immobilised on the graphene oxide surface. APTMS and graphene oxide both being hydrophilic in character are blended to give a homogenous dispersion. It is known that the residual groups of the organofunctionalised silane (APTMS) and the oxygen

functionalities act as the active sites for the nucleation of Au/GO nanocomposites. APTMS has been proven to be a versatile capping agent for the Au^{3+} ions, (Pandey and G. Pandey, 2014a) holding a precise control over the nucleation of gold nanoparticles and Au^{3+} ions to ensure they get individually hooked up at the oxygen moieties on the graphene surface, (Cui et al., 2015) as reported in the literature. Thus, both the groups facilitate the regulation of the sizes of the in situ budding nanoparticles over the graphene surface. As evident from the UV-Vis and the transmission electron microscopy data, the size of the fabricated gold nanoparticles is relatively small, and the zeta potential measurements, as discussed later, ensure the stability of the Au/GO dispersion. The synthetic procedure for Au/GO nanohybrids is compared with that of the AuNPs synthesised without GO. The gold nanoparticles wrapped with GO are formed within a shorter span of time, comparatively. The kinetics of the sonochemical synthesis of AuNPs and Au/GO nanohybrids were recorded and are shown in Figure 3.16.

The concentrations of the reactants were kept constant, and the time-dependent formation of AuNPs was studied in the absence (Figure. 3.16a-b) and the presence of 1 mg mL^{-1} GO (Figure. 3.16c-d). The variation in absorbance as a function of time is shown in the form of bar diagrams, and confirmed that GO promotes the rate of AuNPs formation under similar conditions. The reasons for such variation may be further explained as follows. The synthetic procedure for Au/GO nanohybrids is compared with that of the AuNPs synthesised without GO. The gold nanoparticles wrapped with GO are formed within a shorter span of time, comparatively. The kinetics of the sonochemical synthesis of AuNPs and Au/GO nanohybrids were recorded and are shown in Figure 3.16. The concentrations of the reactants were kept constant, and the time-dependent formation of AuNPs was studied in the absence (Figure 3.16a-b) and the presence of 1

mg mL^{-1} GO (Figure 3.17c-d). The variation in absorbance as a function of time is shown in the form of bar diagrams, and confirmed that GO promotes the rate of AuNPs formation under similar conditions. The reasons for such variation may be further explained as follows. The micellar behaviour of APTMS is responsible for the controlled morphology and sizes of the nanoparticles (Pandey and Pandey, 2014).

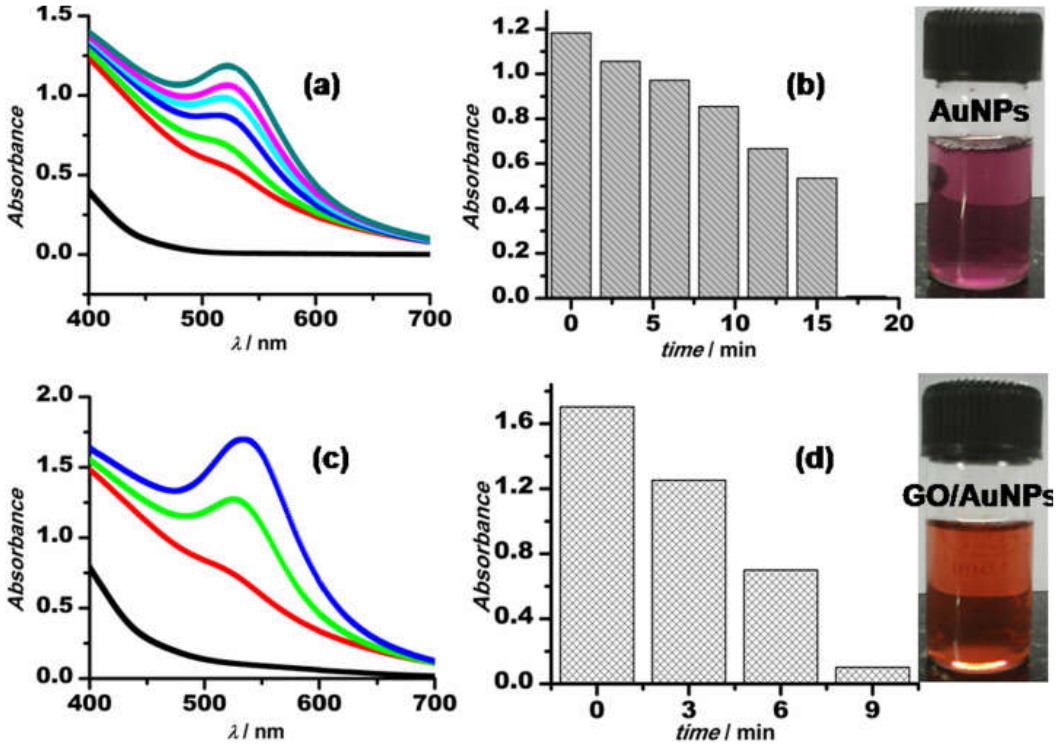

Figure 3.16. Variation in absorbance spectra of synthesis of a). AuNPs and c). GO-AuNPs. Bar daigrams c) and d) representing the increase in absorbances recorded in relation to time.

Graphene (GO) sheets act as a supporting material for the dispersion of metal nanoparticles, and due to the presence of a number of functional groups containing "O" heteroatom with lone pairs, which configures the non-bonding interactions with the charged metal ions, are also accountable for the controlled nucleation of the nanospheres and for preventing the nanoparticles becoming

in close proximity to coalesce. This inference is supported by the stability studies carried out by zeta potential measurements (Lombardi and Birke, 2008).

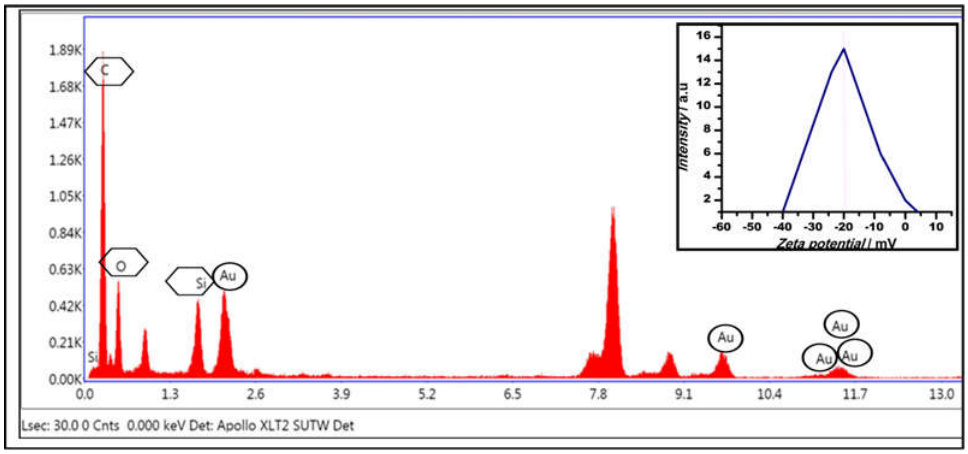

Figure 3.17. EDS spectrum of Au-GO nanocomposite. Inset figure gives the zeta potential of the Au-GO nanocomposites.

The zeta potential of Au/GO nanocomposite was found to be near about 25 mV (Inset, Figure 3.17), which shows that the prepared nanohybrid is significantly stable, and has a relatively better shelf-life than the homogeneous suspension.

3.4.4. Structural analysis of AuNPs

Interpretation of the HRTEM micrographs (Figures 3.13d and 3.14) show a consistent, non-overlapping and dense distribution of individual gold nanocrystals over the surfaces of graphene oxides. This ensures the non-aggregation of the particles at any site and thereby justifies the promotional effect of graphene oxide on the morphology and structural arrangement of AuNPs. Furthermore, the nanoparticles do not coalesce into one another to form bigger particles, which prove the significant roles of APTMS and the oxygen functionalities. The prepared nanohybrids

were considerably smaller, which is in agreement with respect to the statistical data available from previous studies, (Cui et al., 2015; Sun et al., 2015) where the reported nanoparticles are above 20 nm in diameter. This demonstrates that the synthetic route followed here generates a material with superior quality over the conventional pathways reported earlier (Cui et al., 2015; Sun et al., 2015). The polydisperse character of Au/GO is well indicated by the variation in sizes of the nanocrystals and corresponding lattice spacings. The selected area electron diffraction (SAED) patterns, as shown in Figure 3.13a, provide a deeper insight into the crystallographic structure of the materials. Further surface analysis of the nanocomposites was performed using energy dispersive X-ray spectroscopy (EDX). The spectra obtained (Figure 3.12) give information about a number of constituent materials, such as carbon (skeleton of graphene), oxygen (functional groups), Si (organosilane) and Au (nanoparticle), present in the prepared nanohybrids. Table 3.2 presents the Au content in the Au/GO nanohybrids.

Table 3.2. Content of Au and other constituents in Au/GO nanohybrids

Element	Weight %	Atomic %
C K	65.86	72.47
O K	32.32	26.70
Si L	1.67	0.78
Au L	.15	0.05

3.4.5. Hydrogen evolution from Hydrazine

The trend of catalytic hydrogen evolution so obtained, follows the order: Pd/GO/EETMS (623 K)> Pd/GO/EETMS (423 K) > Pd/GO/EETMS> Pd/GO/GPTMS > Pd/EETMS > Pd/GPTMS.

Heat treated catalysts, i.e., Pd/GO/EETMS is found to be highly active toward the decomposition of hydrazine as compared to others justifying the effect of the surface properties for the activity and selectivity of the catalysts (Wang et al., 2012; Yang et al., 2009). The decomposition of hydrazine is expected to follow the proposed mechanism, reported in scheme 3.4 based on the FTIR studies.

Pd/EETMS is more efficient than the Pd/GPTMS, because Pd/EETMS has exceptionally better crystallinity properties as clear from the SAED patterns (Figure 3.3b), whereas the nanoparticles synthesized using GO are examined to have desirable catalytic activity due to homogenous distribution of the nanoparticles over the graphene surfaces along with the polymeric matrix induced dispersion. In that Pd/GO/EETMS is even faster than the Pd/GO/GPTMS, due to broad differences in their sizes. Later one being bigger in size (21.5 ± 7.4 nm), as compared to Pd/GO/EETMS (3.41 ± 0.9 nm), thus less effective toward the decomposition of hydrazine. Pd/GO/EETMS when treated at elevated temperatures (423 and 623 K), acts as highly potential catalysts with improved efficiencies. Dissolved hydrogen was estimated using methylene blue (MB), as it reacts with equimolar concentration of dissolved hydrogen in solution, and transforms to colorless reduced form i.e., leucomethylene blue (leucoMB) (Tafreshi et al., 2015), allowing the convenient assessment of the amount of hydrogen released corresponding to different catalyst added under similar conditions. MB has an absorption maxima at 290 and 662 nm, the band in visible region (at 662 nm) disappears on conversion to leucoform, therefore the reaction dynamics is easily studied by UV–Vis spectroscopy (Figure 3.11a). Present TOF (h^{-1}) values for the decomposition of hydrazine are compared with those of Pt and Ni based catalysts which are good catalysts, yet less efficient than the immobilized catalyst (Tafreshi et al., 2015).

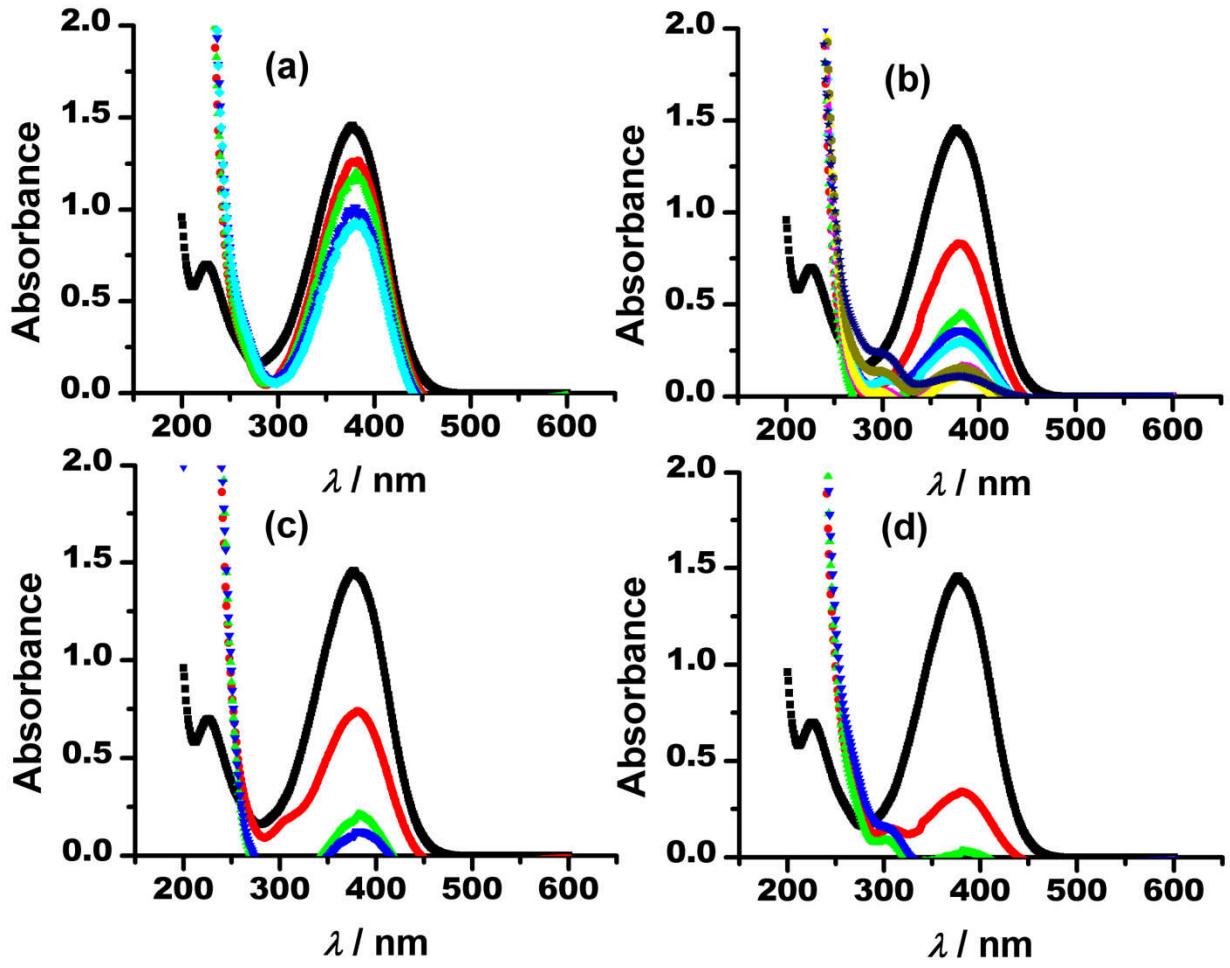

Figure 3.18. Absorbance spectra of p-nitroaniline reduction using (a) Pd/GPTMS, (b) Pd/EETMS, (c) Pd/GO/GPTMS, and (d) Pd/GO/EETMS. Solid line represents the p-nitroaniline.

Further, the kinetic analysis (Figure 3.11b) inferred that the heat treated catalyst (Pd/GO/EETMS at 623 K) is more efficient. The silica alginate bead encapsulated palladium nanocomposites are used as effective heterogenous catalysts for the evolution of hydrogen in the reduction of p-nitroaniline (PNA) (Seo et al., 2012; Pozun et al., 2013). The absorbance maxima of PNA lie at 400 nm and on reduction to p-diaminobenzene, it is shifted to 310 nm, this blue shift in wavelength can be monitored conveniently.

Relative rates of reduction reactions for all the catalysts (Pd/EETMS, Pd/GO/EETMS, Pd/GPTMS, Pd/GO/GPTMS) are recorded using UV–Vis spectroscopy as shown in Figure 3.18. The slopes of the plots of natural logarithm of the variations in absorbance against time, yields apparent rate i.e., kapp. At regular intervals the absorbance was recorded (At, absorbance at different periods, while A_0 is initial absorbance) and the graphs were plotted, from where slope was obtained (kapp). The rate constants were calculated at 298 K for Pd/GO/EETMS, with and without heat treatments.

The values of slopes are 0.271 min^{-1} (4.5 x 10^{-3} s^{-1}) 0.428 min^{-1} (7.1 x 103 s^{-1}), and 1.03 min^{-1} (17.1 x 103 s^{-1}) for Pd/GO/EETMS, Pd/GO/EETMS (423 K), and Pd/GO/EETMS (623 K) respectively in comparison to the earlier reports where Pt (4.6 x 10^{-4}), (Kocak et al., 2016) Au/PMMA (7.2–7.9 x 10^{-3}), (Park et al., 2009) PAA/Ag (0.3 6 0.1) (Kuroda et al., 2009). The highest value of slope is obtained for Pd/GO/EETMS (623 K), which is comparable to the values calculated so far for Pd based catalysts. Absorbance spectra were recorded with the subjection of catalysts and hydrazine (100 μL, 1.19 M), using the aliquots from the undergoing reactions. The reactions took 65, 40, 30, 10 min in case of Pd/GPTMS, Pd/EETMS, Pd/GO/GPTMS, and Pd/GO/EETMS as evident from the bar diagrams (Figure 3.19) representing the variations in absorbance relative to time. Basis of these deviations are the same, as explained earlier. The fine pore sizes of the silica beads encapsulated with Pd/GO/EETMS nanocomposite, lead to the fast interaction with the PNA molecules, resulting in the rapid chemical change. The order of the catalytic aptitude achieved is Pd/GO/EETMS > Pd/GO/GPTMS > Pd/EETMS> Pd/GPTMS.

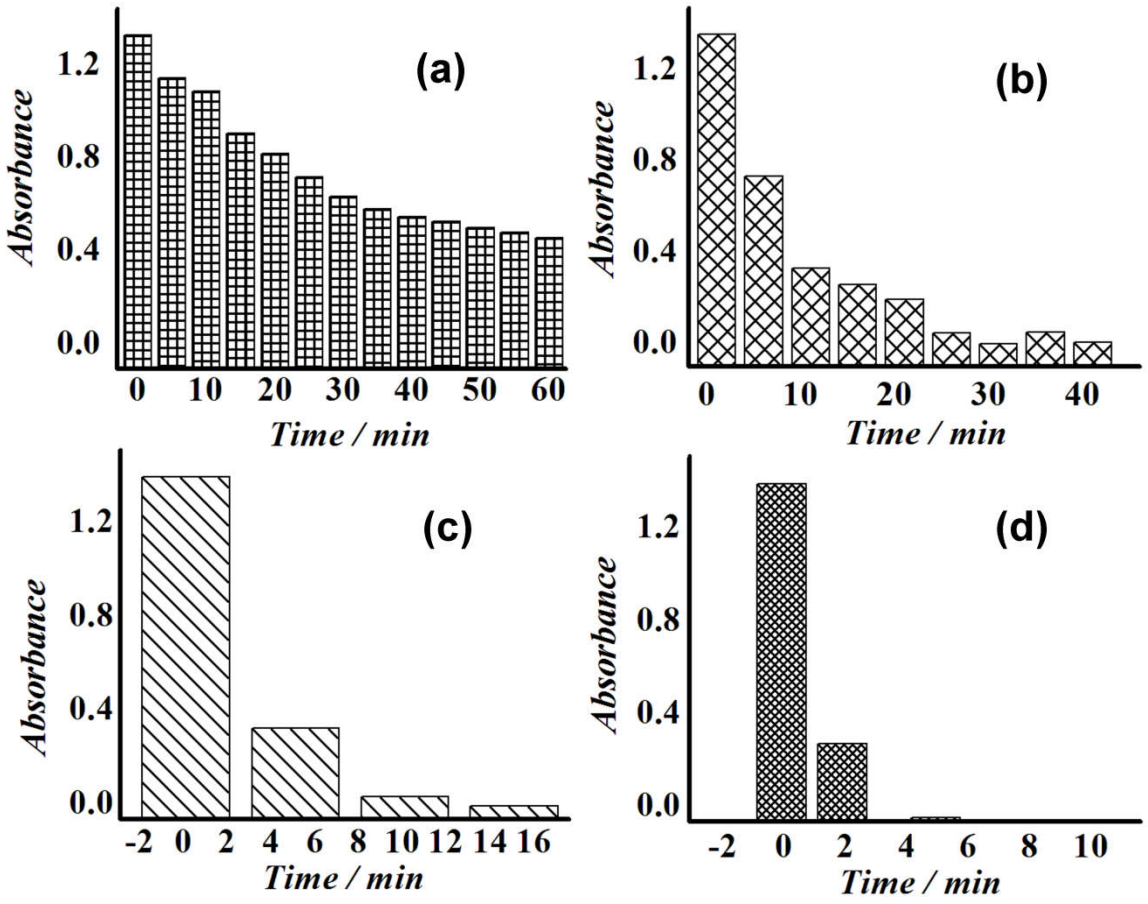

Figure 3.19. Bar diagrams representing the variation in absorbance and completion of reaction, in relation to time for (a) Pd/GPTMS, (b) Pd/EETMS, (c) Pd/GO/GPTMS, and (d) Pd/GO/EETMS.

3.4.6. Catalysis at elevated temperatures

The technology of encapsulation of nanomaterials into the silica alginate beads further extends the possibilities of their conversion to highly competent materials for catalysis. The advantages of such transformations include the modification of the colloidal dispersion of palladium nanoparticles into the even more, dynamic configuration, accountable for its wider access towards high catalytic activity. On the other hand, it is immensely challenging and arduous technique to remodel the colloidal dispersion of palladium nanoparticles into powdered

palladium metal profile, as their treatment at elevated temperatures generally mutates the nano-geometry. On treatment at elevated temperatures, tailored the properties, for instance, the crystallinity of the material was enhanced (Kuroda et al., 2009) to a much higher extent. The modified material responds even faster toward the decomposition of hydrazine (Figure 3.8d), conversion of MB to leucoMB, reduction of p-nitroaniline to p-diaminobenzene (Figure 3.20).

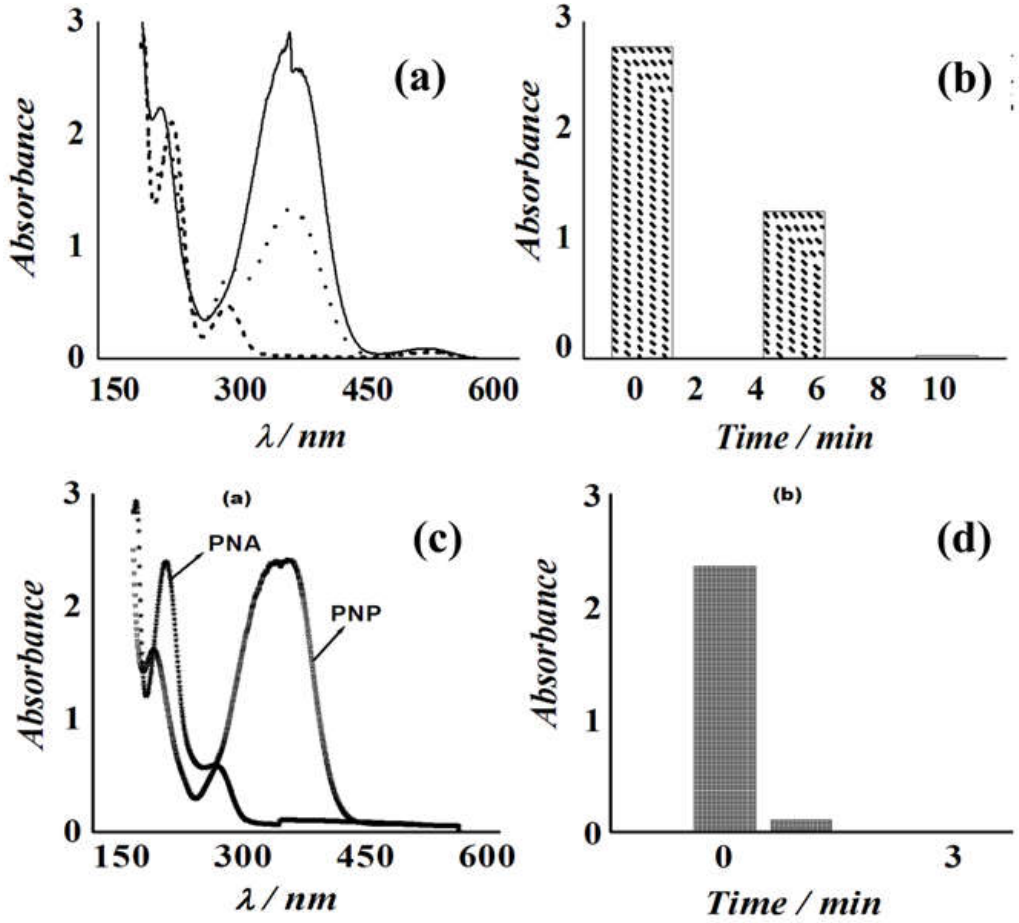

Figure 3.20. Absorption spectra of reduction of p-nitrophenol using heat treated catalyst (a) at 423 K and (b) 623 K and corresponding bar diagrams (c) and (d).

3.4.7. Stability and recyclability studies

Silica-alginate beads before and after heat treatments are compatible to recycling, i.e., these can be regained from the reaction mixture and can be applied to another cycle of experiments, hence they are highly cost effective. These are found to retain, splendid catalytic potential irrespective of being used in a recurring manner for successive set of operations.

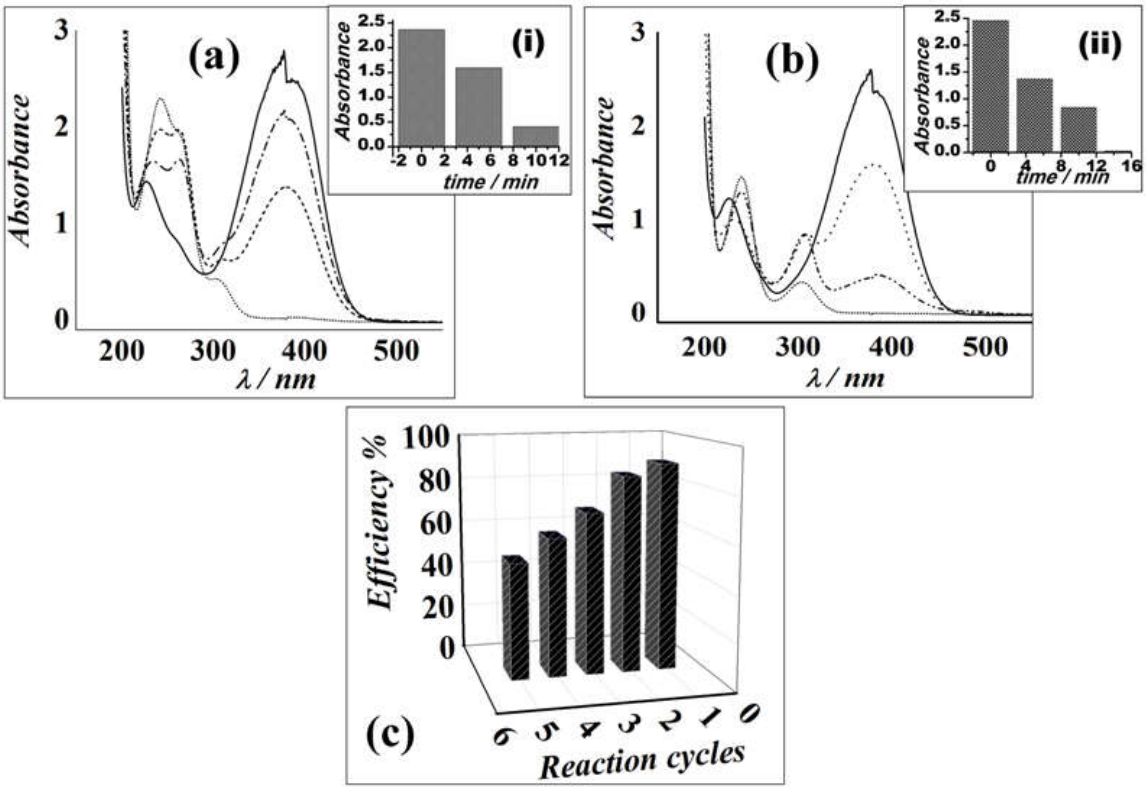

Figure 3.21 Stability test before (a) and after 5–6 days (b), (i) and (ii) represent the variation in absorbance relative to time (c) recyclability assessment over 5 experimental cycles for the silica alginate beads entrapped with nanocomposites. Stability and recyclability was examined through p-nitroaniline reduction with 1.19 M hydrazine.

Figure 3.21 shows the efficiency of the catalyst (silica alginate bead with Pd/GO/EETMS nanocomposite) used over 4–5 experimental cycles. Appreciable activity of the catalysts was

observed over successive cycles, retaining about 80% of its activity even after 5 cycles, which defines its fair catalytic accessibility. The same catalyst was studied for its stability toward the release of hydrogen and in turn reduction of nitro compound (PNA) over 5–6 days. Figure 3.21 a–b shows the similar activity after 5–6 days.

3.5. CONCLUSIONS

A novel and highly effective methodology to fabricate the mesoporous silica alginate beads with precisely controlled pore sizes (2–10 nm) has been demonstrated in this chapter. Graphene oxide (GO) and EETMS functionalized palladium nanoparticles are introduced into the polysaccharide matrix of alginate hydrogel to form silica modified microspheres, with controlled hydrophilicity and improved rigidity. The fabricated composites have exceptionally tunable catalytic properties and were utilized as heterogeneous catalysts, specifically for hydrogen evolution from the decomposition of hydrazine. Out of different systems (silica beads encapsulated with Pd/GPTMS, Pd/EETMS, Pd/GO/GPTMS, and Pd/GO/EETMS), one with Pd/GO/EETMS nanoparticles, is found to be highly active material, justifying the role of alkoxysilane in improving the properties of the materials. When treated at elevated temperatures, silica beads with Pd/GO/EETMS nanoparticles attained mesoporous framework with enhanced rigidity and are found to exhibit the highest level of catalytic activity. This miniatured machinery can be reliably adopted for various other applications. Also, graphene oxide accelerates the synthesis of gold nanoparticles. Graphene oxide and APTMS have a mutual control over the particle size and do not permit agglomeration. APTMS acts as a surface modification and capping agent while GO sheets provide nucleation sites for the gold nanoparticles to grow over the surface. These miniatured machineries can be reliably adopted in various other practical applications.